Materials Research Proceedings 41 (2024) 2134-2143 https://doi.org/10.21741/9781644903131-235

Fatigue resistance of deep drawn parts: A scale bridging simulative study using representative volume elements and crystal plasticity simulations

FEHLEMANN Niklas[1,a*], HENRICH Manuel[1], MÜLLER Martina[2], KÖNEMANN Markus[1], BERGS Thomas[2,3], MÜNSTERMANN Sebastian[1]

[1]Institute of Metal Forming, RWTH Aachen University, Intzestraße 10, 52072 Aachen, Germany

[2]Manufacturing Technology Institute MTI of RWTH Aachen University, Campus-Boulevard 30, 52074 Aachen, Germany

[3]Fraunhofer Institute for Production Technology IPT, Steinbachstraße 17, 52074 Aachen, Germany

[a]niklas.fehlemann@ibf.rwth-aachen.de

Keywords: Deep Drawing, Fatigue, Representative Volume Elements, Crystal Plasticity

Abstract. The mechanical properties of formed components are determined by the interaction between the microstructure and the load path of the forming process. To investigate and understand these effects, micromechanical simulation concepts can be used, such as statistically Representative Volume Elements (sRVE) coupled with crystal plasticity simulations. This study presents a concept that uses sRVE simulations to quantify the influence of three different deep drawing load paths on the fatigue resistance of DP800 steel. The first step is a scale-bridging simulation approach that employs macroscopic simulations of the deep drawing process to extract the boundary conditions for the sRVE simulations with Damask. Subsequent cyclic loading is then simulated. 50 sRVE are computed for each load path to estimate fatigue resistance based on a Fatigue Indicator Parameter. The results indicate that fatigue resistance increases with increasing deformation-induced strain hardening. Additionally, a positive correlation between the martensitic ligament structures and fatigue resistance was observed.

Introduction

To achieve Europe's' ambitious climate goals [1], it is increasingly necessary to design and construct structural components more efficiently. This requires continuous improvement of manufacturing processes, such as forming processes, in conjunction with the materials used. Several studies have already demonstrated that a well targeted and damage controlled forming process leads to improved component performance and can ultimately unlock lightweight potential [2,3]. In deep drawing, a critical sheet metal forming process, key parameters for modified process control include variables such as blank holder force, drawing velocity, friction, and the radius of the drawing ring [4,5].

To achieve a precise selection and optimization of materials for different manufacturing processes, it is essential to have a fundamental understanding of materials and their microstructures. Simulation methods are often used to achieve this understanding. In microstructure simulation, numerical crystal plasticity (CP) models are frequently used in conjunction with statistically Representative Volume Elements (sRVE), for example for the modelling of complex materials in [6,7]. Bargmann et al. [8] provide a comprehensive overview of the various methods for generating and applying sRVE. They offer a significant advantage in that they allow for the independent investigation of individual microstructure components, which can be experimentally challenging and often impractical [9]. Pütz et al. [10] quantified the influence of martensitic band structures in DP800 steel on the initiation of martensite fracture

under bending loads using statistically representative volume elements (sRVE). In addition, the study found that the influence is depending on the phase contrast.

When optimizing component design, it is important to consider not only the forming process but also the load boundary conditions of the component application in the next step. Many parts and components are subjected to cyclic loads, and as a result, almost 90% of all component failures can be attributed to fatigue phenomena [11]. For accurate modelling of fatigue, the representation of the underlying physical mechanisms is crucial, which therefore makes crystal plasticity models paired with sRVE a method of choice [12]. Experimental investigations have shown that fatigue cracks frequently occur at persistent slip bands (PSBs) [13,14]. Based on these underlying physical mechanisms, various so-called Fatigue Indicator Parameters (FIPs) can be derived and used for prediction of the fatigue lifetime based on simulative results [15].

In this paper we present a simulation concept for the evaluation of fatigue life. Within this concept, the effects of the microstructure of a material as well as those of the load path before fatigue can be considered. The fatigue resistance of differently deep-drawn parts, such as seat rails, is used to demonstrate this concept. The aim is to gain a better understanding of the interaction between the complex strain paths during the manufacture and component in-use with the microstructure.

Materials and Methods

The approach presented in this study is based on three distinct steps. First, a geometric reconstruction of the material to generate sRVE. Secondly, an approach for transferring the load paths of the macroscopic forming simulation to the sRVE and third, a methodology for the material simulation and the subsequent estimation of the fatigue resistance.

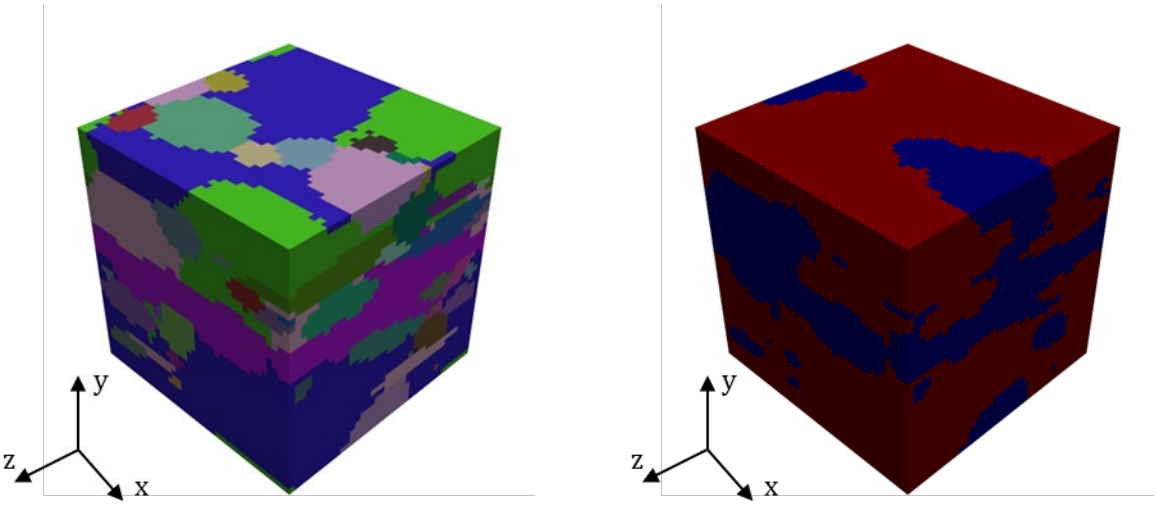

Figure 1: Exemplary sRVE with martensite band (oriented along x- and z-direction) used in this study. Left: Representation of the individual grains (the colors are only an indicator for the individual grains, they do not correspond to a specific orientation). Right: visualization of the different phases (martensite: blue, ferrite: red)

Material reconstruction. The example material in this study is a commercially available dual-phase steel DP800. The material was already extensively characterized in various previous studies, especially the complex micromechanical behavior of the material [16–18]. The used sRVE from the material were created using the AI-supported sRVE-generator DRAGen [19,20], developed by the author's group. This generator can reconstruct the morphology of the microstructure with greater accuracy than conventional methods, including the distinct martensitic banded structures that frequently occur in dual-phase steel grades. For these steels in particular, an accurate

representation of the microstructure is important for a correct modelling of the mechanical properties [21]. For more details on the underlying generation mechanisms in the generator, the reader is referred to Henrich et al. [20]. A total of 50 statistically representative volume elements (sRVE) were generated, evenly distributed between 25 specimens featuring martensite bands and 25 without. To maintain statistical representativeness while simultaneously managing computational costs, a size of 20x20x20 μm was chosen. In this context, 1 μm was discretized into 2 points, resulting in an edge length of 40. The martensite content was specified at 30%. The ultimate martensite content of the sRVE was determined as 31.2 ± 2.3 %, the slight differences arise from the discrete sRVE-generation process. The configuration of martensite bands adhered to data from a referenced source [22]. Figure 1 provides a representative depiction of an sRVE featuring a martensite band. The left side of the figure shows the grain structure, the right side shows the distribution of the phases. For the sRVE simulation, the spectral solver of the open source framework DAMASK [23] is used.

Macroscopic simulation approach. To seamlessly transpose the boundary conditions of a forming process onto the sRVE in the subsequent step, a suitable scale bridging modeling approach becomes necessary. As an illustrative application, deep drawing with varied drawing die radii r_D

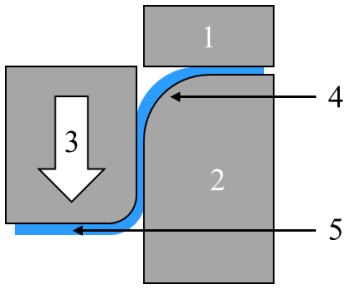

1. Blank Holder
2. Die
3. Punch
4. Die radius r_D
5. Sheet material

Figure 2: Schematic structure of the deep drawing process. Figure adapted from [4].

is considered, as detailed in [4] and depicted in Figure 2. Different drawing ring radii of 3, 6 and 9 mm were selected as exemplary process variations. To enable the transfer of boundary conditions, a specific element in a region of interest within the macroscopic simulation model must be chosen. Depending on the goals of the investigation, this selection can be based on various criteria, such as the element with the highest equivalent plastic strain or von-Mises equivalent stress. Alternatively, a specific location on the component may serve as a reference element for extracting the boundary conditions. In this study, the criterion chosen was the maximum equivalent plastic strain at the end of the load path, aimed at examining the impact of distinct strain hardening behavior on the fatigue properties. It is noteworthy that the element is not constant, it varies with different die radius. Due to the different simulation codes employed for macroscopic (Abaqus/CAE) and microscopic (Damask) simulations, the conventional Abaqus internal submodelling method for transferring boundary conditions is ruled out. Consequently, an explicit user-defined subroutine (VUMAT) is utilized to perform the elasto-plastic simulation of deep drawing, generating the deformation gradient as an output. The nine components of the deformation gradient serve as a load case for the Damask simulation, comprehensively characterize the load path. As a simplification, the entire forming process is assumed to occur at a constant strain rate of 0.001 1/s, owing to the unavailability of strain rate-dependent material parameters for the sRVE-simulations. Nonetheless, given the uniform speed at which all deep drawing tests are conducted, the impact of this simplification is anticipated to be minimal.

Microscopic simulation approach. The complete load path for the simulation is as follows: First, the sRVE is loaded according to the load path of the deep drawing. The sRVE is then relieved so the homogenized macroscopic stress drops to zero and only residual stresses remain in the

microstructure. Finally, the sRVE is cyclically loaded in a strain-controlled manner with an amplitude of 0.5% for 10 cycles.

A crystal plasticity model is used to map the mechanical behavior of the ferrite. Given the unavailability of valid information about the crystallographic orientations in the martensite due to the unresolved very small substructures in the used sRVE, the martensite is assumed to exhibit isotropic plasticity. The model employed for this purpose is also accessible in Damask, and its formulation closely resembles the crystal plasticity model utilized [23]. The parameters for DP800 were taken from a prior publication and are listed in Table 1:

Table 1: Material model parameters used for ferrite and martensite for DP800.

Phase	N_{Slip}	$\gamma_{slip}\,(-)$	$a\,(-)$	$n\,(-)$	$\xi^0_{Slip}\,(MPa)$	$\xi^{inf}_{Slip}\,(MPa)$	$h^0_{Slip-Slip}\,(MPa)$
Ferrite	24	0.001	4.5	5	150	400	625
Martensite	--	0.001	1.25	30	250	750	2500

The fatigue modeling approach adheres to the methodologies outlined in Gillner et al. and Henrich et al. [12,24]. The critical parameter in this context is the plastic slip γ_{sl} accumulated during cyclic loading, serving as an indicator of dislocation slip and the occurrence of persistent slip bands. Within the framework of crystal plasticity, γ_{sl} is computed based on the plastic velocity gradient (L_p).

$$\gamma_{sl} = \int_0^t \sqrt{\frac{2}{3} L_p : L_p}\, dt \tag{1}$$

The velocity gradient is directly linked to the deformation gradient:

$$\dot{F}_p = L_p F_p \tag{2}$$

In this context, F_p denotes the plastic deformation gradient, and $\dot{F}_p$represents its derivative w.r.t. the time. In the crystal plasticity model embedded in Damask, the plastic deformation gradient is integrated into the multiplicative decomposition of the overall deformation gradient.

$$F = F_e F_i F_p \tag{3}$$

Here, F_e represents the elastic and F_p denotes the plastic component of the deformation gradient. F_i characterizes inelastic strains arising from factors such as damage or phase transformations. The overall deformation gradient F is prescribed as a load path.

After the simulation, the grain-averaged plastic slip is extracted using a python-based postprocessing routine and the maximum is taken over each sRVE. Here, it should be noted that the plastic slip accumulation is only calculated for the cyclic loading, the accumulation during the forming process is not considered:

$$\gamma^{rve}_{sl,max} = \max\left(\frac{1}{N^{gr}_{pts}} \sum_{i=0}^{N^{gr}_{pts}} \gamma_{sl}\right) \quad | \; gr = 1 \ldots N_{gr} \tag{4}$$

The parameters are defined as follows: N_{gr} is the number of grains per Representative Volume Element, N^{gr}_{pts} is the number of points per grain, and γ_{sl} represents the accumulated plastic slip per material point. the averaging process relies on the number of points, which is a common practice in other methods. Consequently, each sRVE yields on specific $\gamma^{rve}_{sl,max}$ value. To accommodate the

scatter in the simulations, the values for each load case are depicted in a histogram, and a right-sided Gumbel distribution is fitted to this data. This approach originates in the weakest link theory [25]:

$$F(x;\mu,\beta) = e^{-e^{\frac{-(x-\mu)}{\beta}}} \tag{5}$$

The parameters μ and β characterize the location and scale of the probability density function (pdf). As per Henrich et al. [24], the product of μ and β results in a Fatigue Indicator Parameter (FIP), offering insights into the material's resistance to fatigue. In general, a high FIP indicates a high probability of fatigue failure and vice versa.

$$FIP = \mu * \beta \tag{6}$$

It is crucial to emphasize that this indicator is purely qualitative and does not offer insights into the actual service life of the material or component. Its suitability lies in comparing various load cases and/or material conditions.

Results

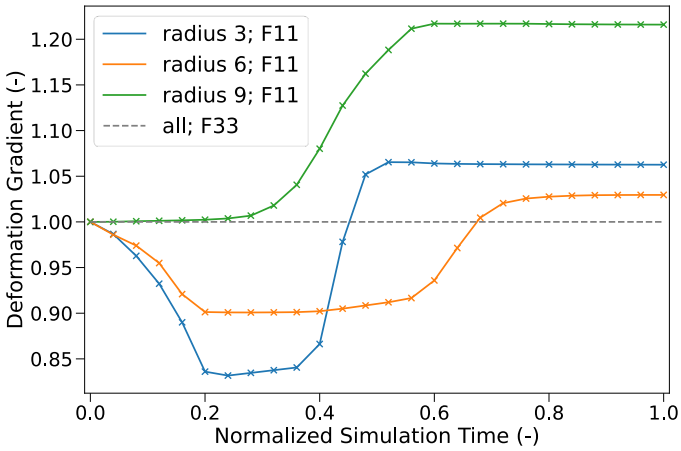

Figure 3: Deformation gradients for all load cases considered. The solid line shows the F11 component (x-direction). The F33 component (grey dashed line) is 1 for all 3 load paths, which means no deformation in the z-direction.

Figure 3 displays the evolution data of the deformation gradients extracted from the macroscopic simulation. The solid lines depict the F11 component of the deformation gradient (x-direction), while the dashed grey line represents the F33 component (z), which is consistently 1.0 for all three load cases, indicating a plane strain state in the respective element. Notably, significant differences in final deformation are evident among various drawing die radii. Specifically, at a radius of 9 mm, the F11 deformation gradient at the end of the load case is around 1.22, contrasting with 1.03 and 1.06 for radii 6 and 9, respectively. The tension-compression load change is more pronounced at radius 3 than at radius 6, and it is observed that shear components of the deformation gradient are relatively low. Therefore, the shear components are not depicted here.

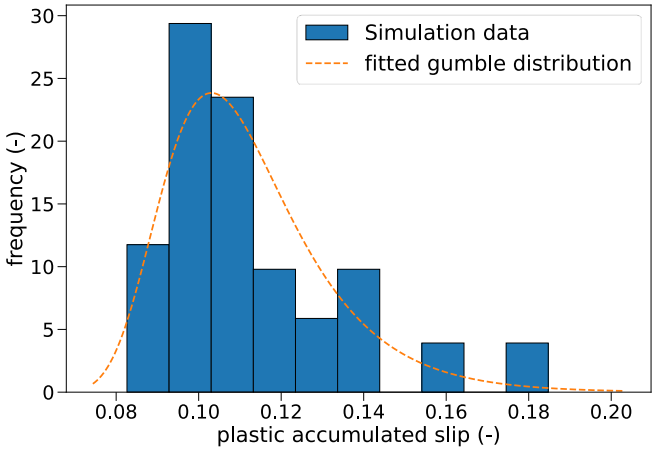

Figure 4: Histogram and fitted Gumbel distribution (orange) for drawing die radius of 3mm.

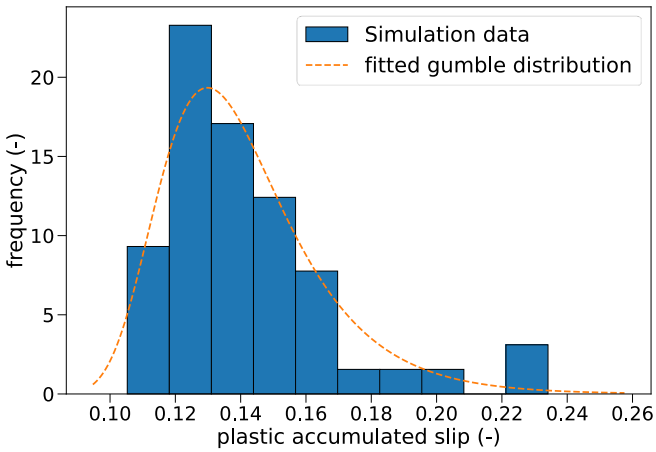

Figure 5: Histogram and fitted Gumbel distribution (orange) for drawing die radius of 6mm.

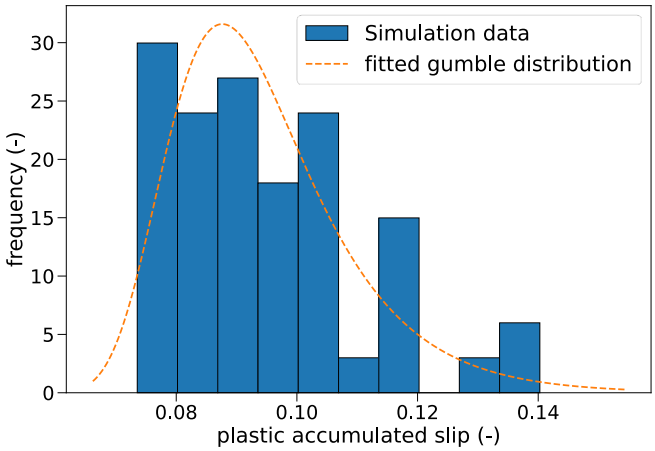

Figure 6: Histogram and fitted Gumbel distribution (orange) for drawing die radius of 9mm.

The different load paths consequently result in distinct fatigue behavior. The figures 4 - 6 depict histograms and fitted Gumbel distributions for the 50 sRVE for all three considered load cases.

Alongside the visual representations in the histograms, the computed fatigue indicators are presented in Table 2. A FIP was calculated for all 50 sRVE and a separate FIP for a subset with and without martensite bands from 25 sRVE each.

Table 2: Fatigue indicator parameter and location and scale parameter of the Gumbel distribution for all three considered load cases.

		$FIP\ (-)$	$\mu\ (-)$	$\beta\ (-)$	No. sRVE
Radius 9mm	All	0.0010	0.0887	0.0117	50
	Bands	0.0009	0.0880	0.0101	25
	No Bands	0.0012	0.0895	0.0130	25
Radius 6mm	All	0.0024	0.1316	0.0182	50
	Bands	0.0017	0.1330	0.0128	25
	No Bands	0.0028	0.1308	0.0210	25
Radius 3mm	All	0.0015	0.1046	0.0144	50
	Bands	0.0012	0.1030	0.0114	25
	No Bands	0.0018	0.1068	0.0166	25

These data indicate that the Fatigue Indicator Parameter for a drawing die radius of 9 mm is significantly lower than that for 3 mm and 6 mm, with a difference of approximately 2.4 times to radius 6 and about 1.5 times to radius 3. This discrepancy is attributed to both a higher average accumulated strain (μ) and increased scatter (β). The differences in the FIP directly correlate with the final equivalent plastic strain of the different load paths, as illustrated in Figure 7. A higher final level of strain hardening leads to a lower FIP. It is also noteworthy that, for all three load cases, the FIP for the subset without martensite bands is higher than for the subset with martensite bands. This is primarily attributed to the higher scatter in the former.

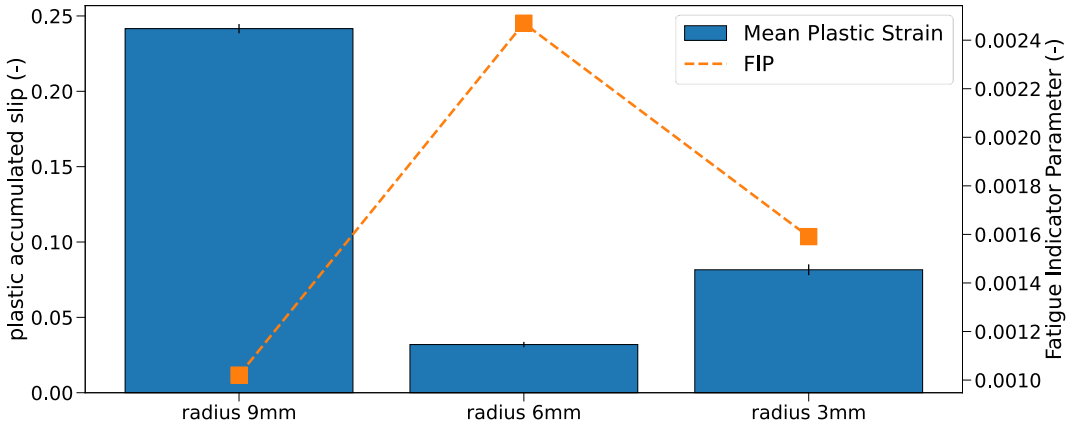

Figure 7: Correlation between Fatigue Indicator Parameter and global equivalent plastic strain, averaged over al 50l sRVE. The FIP tends to decrease with higher strain hardening.

Discussion

The results presented in the preceding section can be analyzed through several stages. Firstly, a distinct correlation between strain hardening and the FIP becomes evident, where higher levels of strain hardening result in a lower FIP and therefore a greater resistance to fatigue. This association is explicable by the fact that, at a higher level of strain hardening, a higher portion of the deformation at the grain level is elastic, thereby reducing the accumulation of plastic slip.

However, it is observed that both the mean strain and the scattering increase with decreasing strain hardening. Experimental studies indicate that scattering tends to increase with an extended fatigue life, which deviates from the observed behavior here. Further investigations are required to elucidate the reasons behind the opposing trends exhibited by the location and scale parameters. It should also be noted that preforming should not be advantageous for parts that are already pre-fatigued. With such parts, non-critical fatigue cracks may become critical. However, as forming from an initial state takes place here, this phenomenon may not be relevant.

A final aspect to discuss is the distinction between the sRVE with and without martensite bands. It becomes evident that the absence of martensite bands primarily results in a higher β parameter, indicating higher scatter. Since a higher proportion of the strain is absorbed by the martensite in the presence of martensitic band structures [10], this can lead to a more homogeneous distribution of strain in the ferrite and therefore less scattering. Therefore, although martensite bands favor the occurrence of ductile damage, they can potentially be beneficial in terms of the fatigue resistance.

Lastly, the analyses presented here does not account for the influence of microscopic damage. In general, micropores may develop - primarily through the fracturing of the hard martensite in the case of the current DP800 - that can also serve as initiation points for fatigue cracks. Given that the distinct load paths are expected to result in varying degrees of damage depending on the drawing die radius [4], the consideration of damage is essential for a more generalized assessment of fatigue resistance. Addressing this aspect can be achieved within the framework of representative volume element simulations, for instance, using suitable phase field models [26], even though acquiring the necessary data for the calibration of these models poses a considerable challenge.

Conclusion

A new simulation concept was presented that uses sRVE simulations and a scalebridging approach to evaluate the effects of microstructure and load path on fatigue resistance. The application of this approach to the fatigue resistance of deep-drawn components made of DP800 with different process parameters revealed a strong dependence of the fatigue resistance on the degree of hardening. It has been demonstrated that the presence of martensitic band structures can positively affect fatigue resistance. Although variables such as deformation-induced damage have not yet been considered, there is a concept available that can be utilized in the design of new materials and manufacturing processes.

Acknowledgements

This research was funded by Deutsche Forschungsgemeinschaft (DFG, German Research Foundation; Projectnumber 278868966 – TRR 188; Damage Controlled Forming Processes, subproject B05 and A06). Simulations were performed with computing resources granted by RWTH Aachen University under project rwth0744.

References

[1] European Commission, European Green Deal. Available at https://commission.europa.eu/strategy-and-policy/priorities-2019-2024/european-green-deal_en.

[2] G. Hirt, A.E. Tekkaya, T. Clausmeyer, and J. Lohmar, Potential and status of damage controlled forming processes, Production Engineering 14 (2020), pp. 1–4. https://doi.org/10.1007/s11740-019-00948-6

[3] A.E. Tekkaya, N. Ben Khalifa, O. Hering, R. Meya, S. Myslicki, and F. Walther, Forming-induced damage and its effects on product properties, CIRP Annals 66 (2017), pp. 281–284. https://doi.org/10.1016/j.cirp.2017.04.113

[4] M. Müller, T. Herrig, and T. Bergs, Numerical analysis of the load paths and the resulting damage evolution during deep drawing of dual-phase steel, IOP Conference Series: Materials

Science and Engineering 1284 (2023), p. 12006. https://doi.org/10.1088/1757-899X/1284/1/012006

[5] P.R. Tiwari, A. Rathore, and M.G. Bodkhe, Factors affecting the deep drawing process – A review, Materials Today: Proceedings 56 (2022), pp. 2902–2908. https://doi.org/10.1016/j.matpr.2021.10.189

[6] F. Qayyum, S. Guk, M. Schmidtchen, R. Kawalla, and U. Prahl, Modeling the Local Deformation and Transformation Behavior of Cast X8CrMnNi16-6-6 TRIP Steel and 10% Mg-PSZ Composite Using a Continuum Mechanics-Based Crystal Plasticity Model, Crystals 10 (2020), p. 221. https://doi.org/10.3390/cryst10030221

[7] D. Reimann, K. Nidadavolu, H. ul Hassan, N. Vajragupta, T. Glasmachers, P. Junker, and A. Hartmaier, Modeling Macroscopic Material Behavior With Machine Learning Algorithms Trained by Micromechanical Simulations, Frontiers in Materials 6 (2019). https://doi.org/10.3389/fmats.2019.00181

[8] S. Bargmann, B. Klusemann, J. Markmann, J.E. Schnabel, K. Schneider, C. Soyarslan, and J. Wilmers, Generation of 3D representative volume elements for heterogeneous materials: A review, Progress in Materials Science 96 (2018), pp. 322–384. https://doi.org/10.1016/j.pmatsci.2018.02.003

[9] J.P.M. Hoefnagels, B.G. Vossen, and C.C. Tasan, Electron Micrographic Digital Image Correlation: Method Optimization and Microstructural banding Case Study, in: Application of Imaging Techniques to Mechanics of Materials and Structures, Volume 4, T. Proulx, ed., Conference Proceedings of the Society for Experimental Mechanics Series. Springer New York, New York, NY, 2013, pp. 71–77. https://doi.org/10.1007/978-1-4419-9796-8_10

[10] F. Pütz, N. Fehlemann, V. Göksu, M. Henrich, M. Könemann, and S. Münstermann, A data driven computational microstructure analysis on the influence of martensite banding on damage in DP-steels, Computational Materials Science 218 (2023), p. 111903. https://doi.org/10.1016/j.commatsci.2022.111903

[11] R.I. Stephens, A. Fatemi, R.R. Stephens, and H.O. Fuchs, Metal fatigue in engineering, 2nd edn. Wiley, |c c2001, New York, 2001.

[12] K. Gillner and S. Münstermann, Numerically predicted high cycle fatigue properties through representative volume elements of the microstructure, International Journal of Fatigue 105 (2017), pp. 219–234. https://doi.org/10.1016/j.ijfatigue.2017.09.002

[13] J. Polák and J. Man, Mechanisms of extrusion and intrusion formation in fatigued crystalline materials, Materials Science and Engineering: A 596 (2014), pp. 15–24. https://doi.org/10.1016/j.msea.2013.12.005

[14] J. Polák, J. Man, T. Vystavěl, and M. Petrenec, The shape of extrusions and intrusions and initiation of stage I fatigue cracks, Materials Science and Engineering: A 517 (2009), pp. 204–211. https://doi.org/10.1016/j.msea.2009.03.070

[15] N. Sayer, E. Natkowski, P. Sonnweber-Ribic, and S. Münstermann, A novel microscale fatigue failure indicator considering plastic irreversibility for microstructure-based lifetime simulation, International Journal of Fatigue 163 (2022), p. 107115. https://doi.org/10.1016/j.ijfatigue.2022.107115

[16] R. Meya, C. Kusche, C. Löbbe, T. Al-Samman, S. Korte-Kerzel, and A. Tekkaya, Global and High-Resolution Damage Quantification in Dual-Phase Steel Bending Samples with Varying Stress States, Metals 9 (2019), p. 319. https://doi.org/10.3390/met9030319

[17] C. Tian, D. Ponge, L. Christiansen, and C. Kirchlechner, On the mechanical heterogeneity in dual phase steel grades: Activation of slip systems and deformation of martensite in DP800, Acta Materialia 183 (2020), pp. 274–284. https://doi.org/10.1016/j.actamat.2019.11.002

[18] M.A. Wollenweber, S. Medghalchi, L.R. Guimarães, N. Lohrey, C.F. Kusche, U. Kerzel, T. Al-Samman, and S. Korte-Kerzel, On the damage behaviour in dual-phase DP800 steel deformed in single and combined strain paths, Materials & Design 231 (2023), p. 112016. https://doi.org/10.1016/j.matdes.2023.112016

[19] N. Fehlemann, Y. Sparrer, F. Pütz, M. Konemann, and S. Münstermann, Influence of synthetically generated inclusions on the stress accumulation and concentration in X65 pipeline steel, IOP Conference Series: Materials Science and Engineering 1157 (2021), p. 12056. https://doi.org/10.1088/1757-899X/1157/1/012056

[20] M. Henrich, N. Fehlemann, F. Bexter, M. Neite, L. Kong, F. Shen, M. Könemann, M. Dölz, and S. Münstermann, DRAGen - a Deep Learning Supported sRVE Generator Framework for Complex Microstructure Models, Heliyon 9 (2023), e19003. https://doi.org/10.1016/j.heliyon.2023.e19003

[21] D. Yan, C.C. Tasan, and D. Raabe, High resolution in situ mapping of microstrain and microstructure evolution reveals damage resistance criteria in dual phase steels, Acta Materialia 96 (2015), pp. 399–409. https://doi.org/10.1016/j.actamat.2015.05.038

[22] N. Fehlemann, A.L. Suarez Aguilera, S. Sandfeld, F. Bexter, M. Neite, D. Lenz, M. Könemann, and S. Münstermann, Identification of Martensite Bands in Dual-Phase Steels: A Deep Learning Object Detection Approach Using Faster Region-Based-Convolutional Neural Network, steel research int. 94 (2023). https://doi.org/10.1002/srin.202200836

[23] F. Roters, M. Diehl, P. Shanthraj, P. Eisenlohr, C. Reuber, S.L. Wong, T. Maiti, A. Ebrahimi, T. Hochrainer, H.-O. Fabritius, S. Nikolov, M. Friák, N. Fujita, N. Grilli, K. Janssens, N. Jia, P. Kok, D. Ma, F. Meier, E. Werner, M. Stricker, D. Weygand, and D. Raabe, DAMASK – The Düsseldorf Advanced Material Simulation Kit for modeling multi-physics crystal plasticity, thermal, and damage phenomena from the single crystal up to the component scale, Computational Materials Science 158 (2019), pp. 420–478. https://doi.org/10.1016/j.commatsci.2018.04.030

[24] M. Henrich, M. Dölz, and S. Münstermann, Development of a Numerical Framework for Microstructure Sensitive Fatigue Life Investigations, in: Volume 2: Computer Technology & Bolted Joints; Design & Analysis, ASME 2023 Pressure Vessels & Piping Conference, Atlanta, Georgia, USA, Jul. 16-21, 2023. American Society of Mechanical Engineers, 2023. https://doi.org/10.1115/PVP2023-106419

[25] S. Beretta and Y. Murakami, STATISTICAL ANALYSIS OF DEFECTS FOR FATIGUE STRENGTH PREDICTION AND QUALITY CONTROL OF MATERIALS, Fatigue Fract Eng Mat Struct 21 (1998), pp. 1049–1065. https://doi.org/10.1046/j.1460-2695.1998.00104.x

[26] P. Shanthraj, L. Sharma, B. Svendsen, F. Roters, and D. Raabe, A phase field model for damage in elasto-viscoplastic materials, Computer Methods in Applied Mechanics and Engineering 312 (2016), pp. 167–185. https://doi.org/10.1016/j.cma.2016.05.006